

Precise Ionospheric Determination and its Application to Real-Time GPS Ambiguity Resolution

M. Hernández-Pajares, J. M. Juan, J. Sanz, *Group of Astronomy and Geomatics, Universitat Politècnica de Catalunya (gAGE/UPC), Barcelona, Spain*

O.L.Colombo, *USRA/NASA GSFC, Maryland, USA, visiting at the Dept. of Electromagnetic Systems, Danish Center for Remote Sensing, Technical University of Denmark, Lyngby, Denmark.*

BIOGRAPHY

Dr. Manuel Hernández-Pajares is associate professor in the Department of Applied Mathematics and Telematics at the Universitat Politècnica de Catalunya. He started working on GPS in 1989 and now he is currently focused on the area of GPS Ionospheric tomography, neural network algorithms and precise radionavigation.

Dr. J. Miguel Juan Zornoza works in the Department of Applied Physics at the Universitat Politècnica de Catalunya as associate professor. His current research interest is in the area of GPS: Tomography of the Ionosphere, data processing strategies and subdecimeter navigation.

Dr. Jaume Sanz Subirana is an associate professor in the Department of Applied Mathematics and Telematics at the Universitat Politècnica de Catalunya. He is working on GPS processing software, Ionospheric tomography with GPS data and real-time precise positioning.

Dr. Oscar L. Colombo works on applications of space geodesy, including gravity field mapping, spacecraft orbit determination, and precise positioning by space techniques, mostly for the Space Geodesy Branch (Code 926) of NASA Goddard Space Flight Center. In recent years, he has developed and tested techniques for very long baseline kinematic GPS, in collaboration with groups in Australia, Denmark, Holland, and the USA. He contributed to this work while on a 6-month stay as visiting professor at the Electro-Magnetic Systems Institute (EMI), Technical University of Denmark.

ABSTRACT

The influence of the ionosphere is one of the main problems in the real-time ambiguity resolution for the carrier phase GPS data in radionavigation, especially with high geomagnetic activity or close to the next Solar Maximum at year 2000. Therefore, it is important to have a precise estimation of the ionospheric delays.

In the first part of this paper we present a comparison at real-time mode, and using only the carrier phase, of the tomographic model with the traditional 1 fixed height layer model, and it is shown the reduction of the error of the absolute, single difference and double differenced ionospheric corrections. Quiet geomagnetic conditions are simulated with the International Reference Ionosphere model, with real geometry for a network of stations at distances of 400-1000 km in North-America.

In the second part we perform an assessment of the proposed real-time tomographic model, feed with real carrier phase data only, and in three situations with different geomagnetic activity. In the moderate and high activity scenarios, the resolution of the widelane double differenced ambiguities is successful for the greatest part of cases (95% for elevations greater than 20 degrees) when the tomographic ionospheric correction is included. In the storm scenario ($Kp \approx 8$), the results are poorest (60%) at times with highest electron content variations (5 TECU in 2 minutes), but they are better than in the case of neglecting the double difference ionospheric correction.

INTRODUCTION

The free electrons distributed in the atmospheric region named ionosphere (between one hundred and thousands km in height) produce a frequency dependent effect on the Global Positioning System (GPS) signals, a delay in the pseudorange and advance in the carrier phase. Its spatial-temporal distribution is correlated with the position of the main ionizant source: the Sun. It is also dependent on the Solar cycle, on events like Traveling Ionospheric disturbances (TID) and in general on the geomagnetic and Space Weather conditions.

Therefore the distribution of free electrons in the ionosphere affects the precise navigation with GPS, and must be taken into account depending on the distance scales:

- Local Area Differential GPS (LADGPS): when the rover

receiver is far from a reference GPS station less than few tens of km (see for example Pratt et al. 1998). The assumption that the ionospheric errors are identical for both stations and fix then the double differenced integer ambiguities in L_1 strongly depends on the geomagnetic activity and possible existence of ionospheric perturbations like TID (Coster et al. 1998).

- Regional Area Differential GPS (RADGPS): Gao et al. (1997) showed that when the dual frequency rover receiver is at distances of few hundred km from the reference network, the double difference of the integer phase ambiguities can be fixed, estimating the ionospheric delay in minimum Solar cycle conditions.
- Wide Area Differential GPS (WADGPS): using the code it is possible to get positioning errors on the order of ones of meters, modeling the ionospheric delay, among other errors like tropospheric delay, for the main observable: the L_1 pseudorange smoothed with the carrier phase. This is fulfilled with networks of stations separated $\simeq 500$ -1000 km (Enge et al. 1996).

The use of the GPS signals on the two frequencies, and gathered from a set of reference receivers, can be used to compute a real-time ionospheric model in the RADGPS and WADGPS scales, to provide the enough precise ionospheric correction to the GPS navigator. Some examples can be found in Hansen et al. 1998 in WADGPS using as the main observable the smoothed pseudorange, and in Colombo et al. 1999 for RADGPS close to the Solar maximum and using the carrier phases.

The purpose of this paper is, first, to show (with semi-synthetic data) the advantages of using a tomographic model feed with carrier phase data for real time ionospheric modeling (next section). And, second, to evaluate with real data the performance of this model to fix the double differences of the phase ambiguities at scales of RADGPS and WADGPS (few hundreds to one thousand km) and at different geomagnetic conditions.

ASSESSMENT OF THE REAL-TIME TOMOGRAPHIC MODEL

It can be assumed that the electron free density can be described as a random walk process on time, that will be estimated in a reference frame (Sun fixed) where it is relatively stationary (variation of $\pm 5\%$ during one day with low geomagnetic activity¹). The tomographic model adopted is spatially formed by a set of cells or volume elements (voxels), especially suitable to detect local features, that cover all the sampled ionosphere by the GPS rays. In these voxels the electron density is considered constant at a given time. Despite other possibilities to choose the voxel distribution (for instance adapted to the data density like in Hernández-Pajares et al. 1997a) the regular distribution is adequate for describing a region sampled from an approximative homogeneously distributed network of reference stations. A voxel size of 3×5 degrees in latitude and solar longitude, and two layers with

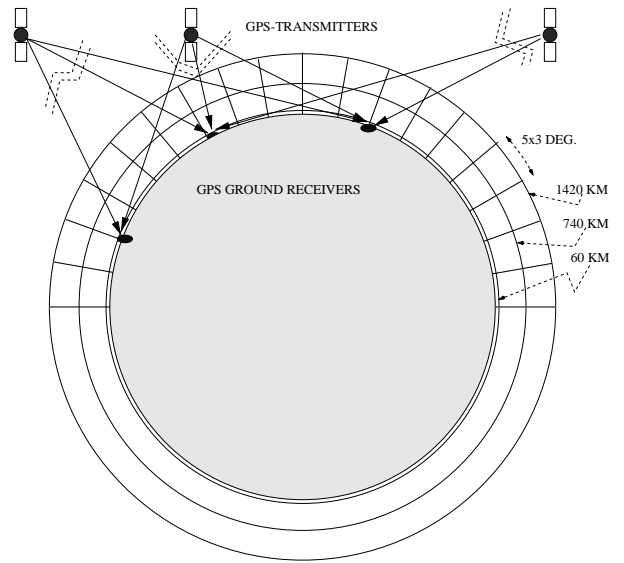


Figure 1: Layout of the two-layer tomographic model adopted to estimate the electron content from reference ground stations.

boundaries at 60-740-1420 km have been adopted (see figure 1). This resolution is adequate to get precise ionospheric determinations from ground GPS data (see for instance Hernández-Pajares et al. 1999).

The resolution of the model, by means of a scalar filter (Bierman 1977) initialized the previous day, is performed from the geometric free combination of phases, $L_I = L_1 - L_2$, of the transmitter T measured from the receiver R (see Colombo et al. 1999 for more details):

$$L_I = \sum_i \sum_j \sum_k (N_e)_{i,j,k} \Delta s_{i,j,k} + b \quad (1)$$

where i, j, k are the indices for each cell corresponding to solar longitude, geodetic latitude and height; $(N_e)_{i,j,k}$ is the corresponding free electron density; and $\Delta s_{i,j,k}$ is the length of the ray path crossing the "illuminated cells"; and b is the alignment term (constant in a given transmitter-receiver arch of continuous phase) that includes the L_1, L_2 integer ambiguities and instrumental delays. This approach extends the model described in Hernández-Pajares et al. (1998).

In order to assess the capabilities of the tomographic model compared to a fixed height thin layer model (at 400 km height), both resolved at real time, we will compare its predictions for absolute, single and double difference slant corrections at distance scales like those of WADGPS.

The data set corresponds to four North-American reference stations belonging to the International GPS Service (IGS) network with distances between 450 and 1300 km (CME1, GOBS, HOLB, WILL). The dual frequency GPS observations, with a sampling period of 30 seconds, are the inputs of the real time ionospheric models to be compared. Also one test station (PABH) is considered whose slant Total Electron Content val-

¹This has been deduced from the IRI, at the geomagnetic equator - Fortaleza, Brazil-, at the noon and in the last solar maximum, 1990, January 1st.

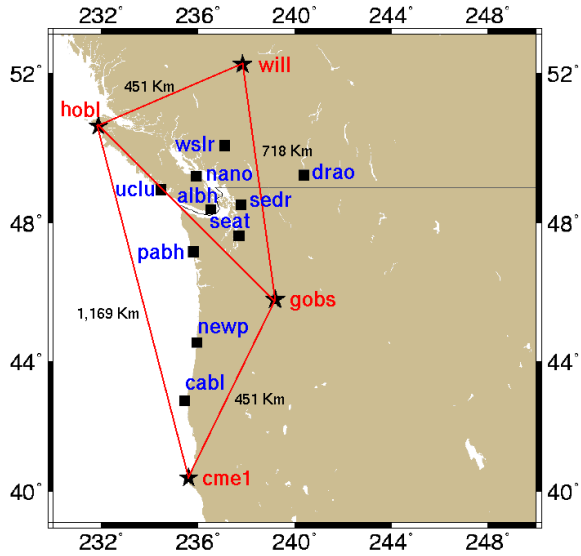


Figure 2: Map of the network of stations used for the study with high geomagnetic activity (stars = reference stations, squares = test stations)

ues (STEC) will be compared to the model predictions (see map in figure 2).

The geometry of the set of observations is the true one for May 3rd, 1998 and the previous day, and the delay values are those predicted by the International Reference Ionosphere (IRI). The observed values taken under high geomagnetic conditions are analyzed in the 2nd part of the paper.

From figures 4 and 3, that summarize the results, and looking at the test station, it is evident that the better results are obtained with the tomographic two-layer model for the absolute, single differenced and double differenced ionospheric correction. This model reduces the errors in a 30-50% approximately compared to the single thin layer model (see table 1 for details). In particular the errors in the double differences of STEC are reduced typically to less than ≈ 10 cm (RMS of 6 cm) in front of the results with the one fixed height thin layer model (≤ 20 cm, with RMS of 9 cm). This is important, as will be discussed in the next section, in order to successfully fix the double differenced integer widelane ambiguity, in particular at the reference stations. And with an accurate strategy for the prediction of the double differenced STEC for the rover receiver, the whole set of ambiguities (of L_1 in particular) can be successfully solved on the fly (OTF). This has been shown during geomagnetically quiet days (that is also the situation simulated with the IRI) and for distance scales of 200-300 km (Colombo et al. 1999).

FIXING THE CARRIER PHASE INTEGER AMBIGUITIES AT DIFFERENT GEOMAGNETIC CONDITIONS

As it has been mentioned above, in the paper from Colombo et al. 1999 the resolution of the carrier phase ambiguities is

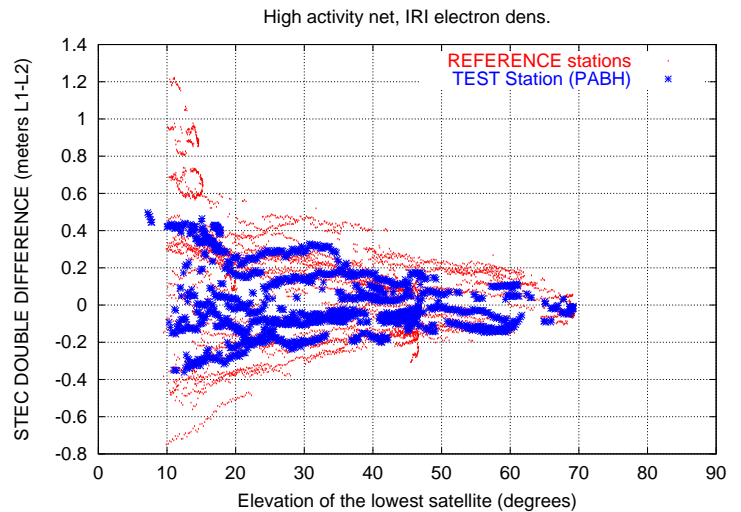
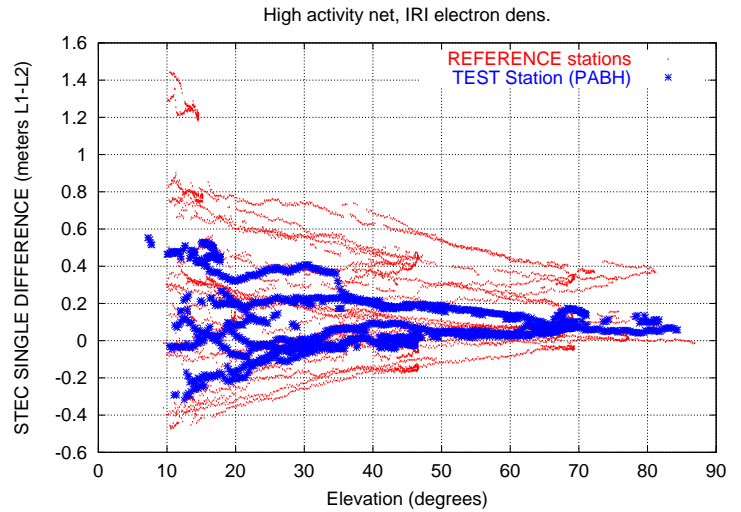
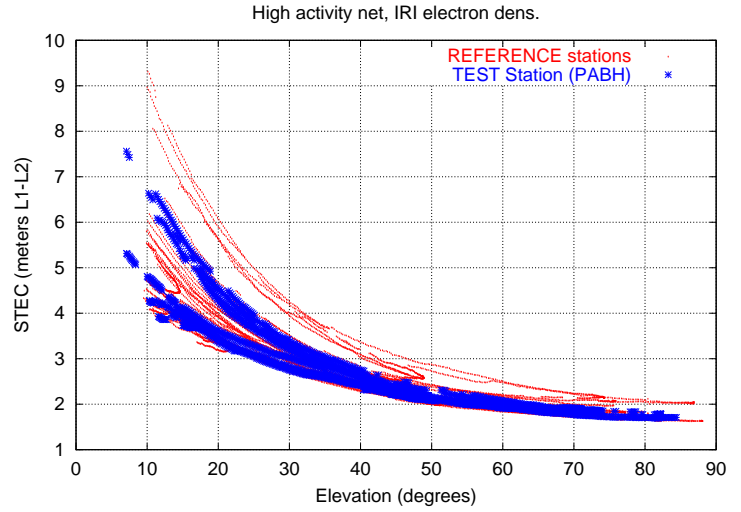


Figure 3: Values modeled for the IRI absolute (top), single difference between stations (middle) and double differenced STEC, for the network studied in the tomographic model assessment.

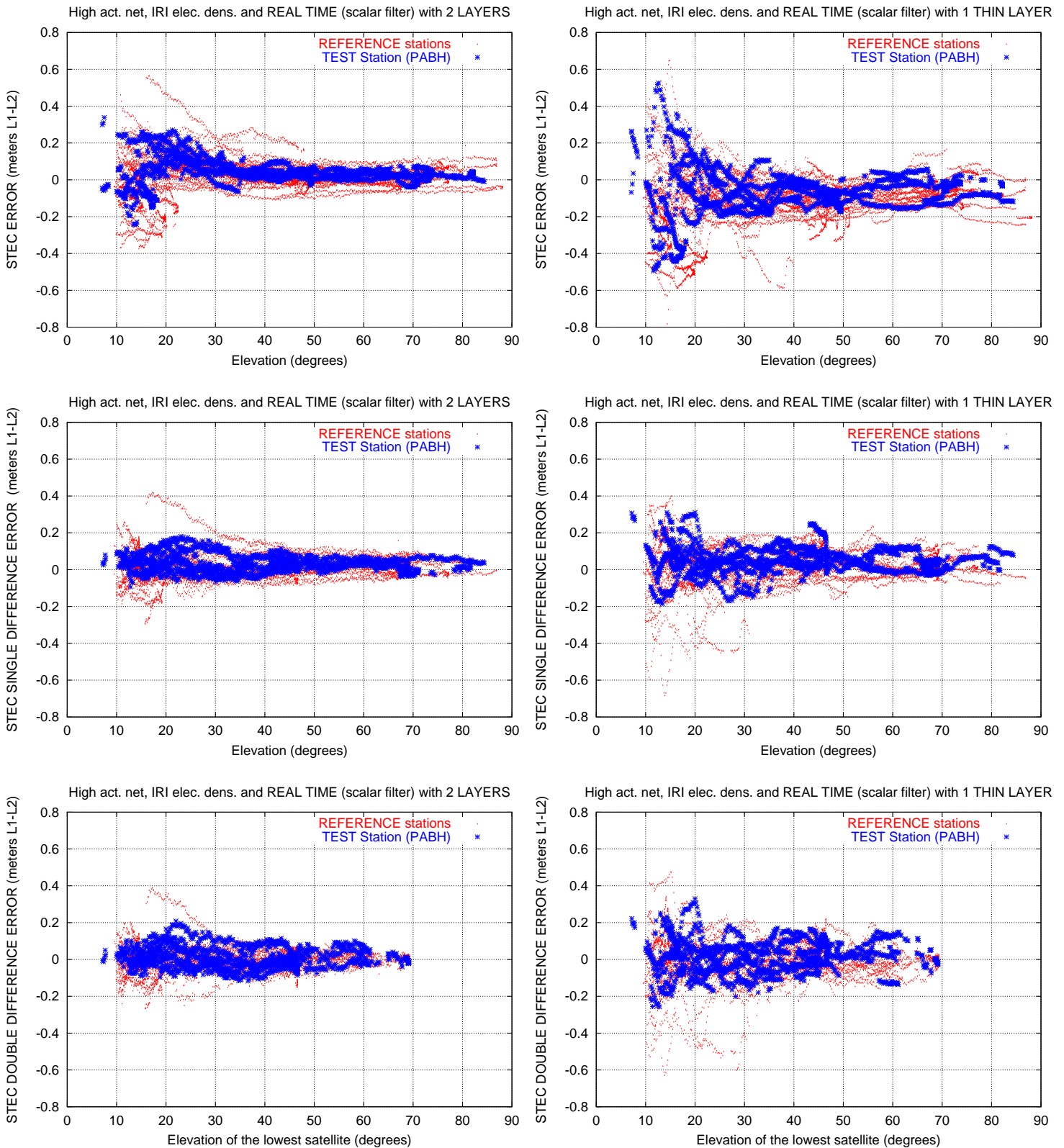


Figure 4: Errors (meters of $L_1 - L_2$ delay) in absolute STEC (1st row), single differenced STEC between stations (2nd row) and double differenced STEC (3rd row), with the two layer model (1st column) and the one thin layer model (2nd column). The green points corresponds to the observations gathered from reference stations (CME1, GOBS, HOLB, WILL) and the red points to the test station PABH (not used in the ionospheric model computation). The geometry corresponds to that of day May 3rd, 1998 with delays simulated with the IRI (more details in the text).

Table 1: Bias, sigma and RMS (meters of $L_1 - L_2$) of absolute, single differenced and double differenced STEC errors (S , ΔS and $\nabla\Delta S$ respectively).

	2 layers model			1 thin layer model		
	Bias	Sigma	RMS	Bias	Sigma	RMS
S	0.04	0.07	0.08	-0.07	0.13	0.15
ΔS	0.03	0.05	0.06	0.05	0.08	0.09
$\nabla\Delta S$	0.01	0.06	0.06	0.02	0.09	0.09

studied for networks of 200-300 km: it is shown the convenience of using a tomographic ionospheric model to solve at real time the ambiguities in the wide-lane combination for the reference stations.

The purpose of the 2nd part of the paper is to assess, for larger networks and higher geomagnetic activity, the capability for solving the double difference of widelane integer ambiguities, by means of the tomographic ionospheric corrections. This is the first step of solving completely the integer ambiguities (also for $L_1 - L_2$ and hence for L_1), studied in the above mentioned paper.

Indeed, if we consider the widelane combination

$$L_\delta = \frac{f_1 \cdot L_1 - f_2 \cdot L_2}{f_1 - f_2} \quad (2)$$

being L_1 and L_2 the carrier phases (in meters) at frequencies $f_1 = 154f_0$ and $f_2 = 120$ ($f_0 = 10.23$ MHz), then its double difference satellite to reference satellite (∇) and station to reference station (Δ) can be written as

$$\nabla\Delta L_\delta = \nabla\Delta\rho + \nabla\Delta T + \nabla\Delta I_\delta + \lambda_\delta \nabla\Delta N_\delta \quad (3)$$

being ρ the distance satellite-receiver, T the tropospheric delay, I_δ the widelane ionospheric correction and N_δ the integer widelane ambiguity (centimetric terms like the phase multipath have been neglected).

To fix OTF $\nabla\Delta N_\delta$ to the right integer value from equation 3 it is necessary to take into account, at real time, the other three terms with a maximum total error less than $\lambda_\delta/2 \simeq 40$ cm, i.e. with an error standard deviation less than $\simeq 20$ cm to guarantee the 95% of successful determination. An error of few centimeters can be expected for the satellite-receiver distance term $\nabla\Delta\rho$, if the satellite positions are obtained from extrapolated precise ephemeris or they are corrected at real time. If the broadcast ephemeris are used instead of, this error term is typically less than 10 cm at distances of 500 km. Regarding to the double differenced tropospheric correction $\nabla\Delta T$, and for stations at distances of few tens of km, the maximum error using the models for the hydrostatic and wet components is typically lower than 10 cm for elevations greater than 20 degrees (this corresponds for a worst case in the study of Coster et al. 1998, figure 5d). But this error can diminish to a few centimeters if the tropospheric correction is estimated at real time, in particular in the reference stations where the coordinates can be accurately known. In our case, using precise orbits and modelled predicted tropospheric corrections, a final maximum error of $\simeq 30 - 40$ cm in $\nabla\Delta I_\delta$ is allowed considering the error budget of the terms in equation 3. This means a standard deviation of ≤ 20 cm for the ionospheric term to guarantee the 95% successful determination of $\nabla\Delta N_\delta$ (i.e.

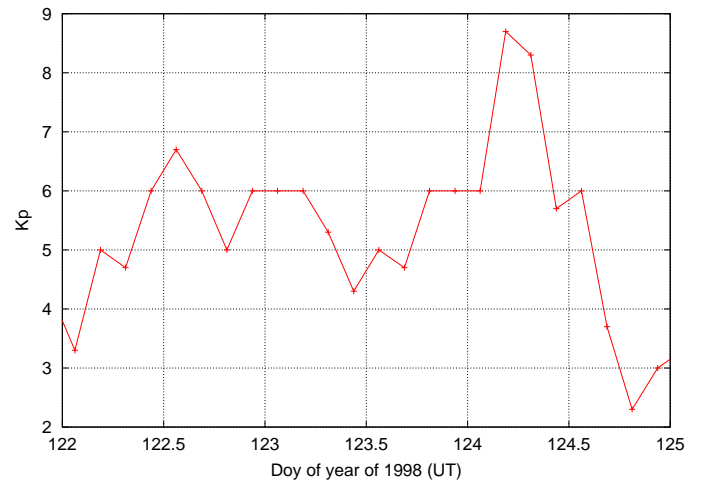


Figure 5: Kp indices for the days 122, 123 and 124 of 1998 (May 2nd, 3rd and 4th), studied in this work

1 TECU or 10 cm in $L_1 - L_2$ delay units approximately).

The study performed in the last section shows us the feasibility to get such precision at real time with the carrier phase tomographic model of the ionosphere during quiet geomagnetic conditions. We are going to study this feasibility with real data under different geomagnetic conditions (see figure 5 with the Kp indices for the involved days).

The different considered networks are formed by IGS stations in the Southwest part of Canada and Northwest of USA. Three scenarios with different geomagnetic conditions are studied, using an ionospheric model similar to that of figure 1 and equation 1:

1. Moderate geomagnetic conditions ($Kp \simeq 3$, May 4th 20-23 UT, close to the noon): With the network of figure 6, whose distances range between 300 and 1100 km. The double differences of the ionospheric model residuals (figure 7) presents a RMS of 9 cm in $L_1 - L_2$ delay units. The widelane ambiguities are successfully solved (compared to the postprocess value aligning the widelane phase with the pseudorange) for more than 95% of the cases with elevations starting at 10 degrees. In contrast, under the assumption of zero ionospheric double difference, i.e. without ionospheric correction, the 95% is only attained for elevations greater than 30 degrees (see figure 8).
2. High geomagnetic conditions ($Kp \simeq 6$, May 3th, 20-23 UT): with reference stations at distances between 450 and 1300 km (see figure 2). The ionospheric double difference residuals presents, like in the moderate geomagnetic scenario, a RMS of 9 cm in $L_1 - L_2$ delay units (figure 9). The 95% approximately of successful widelane integer ambiguities fixing is obtained for elevations greater than 15 degrees in contrast with the minimum elevation of 50 degrees when the double difference ionospheric correction is neglected (figure 10).
3. Large geomagnetic storm conditions ($Kp \simeq 8$, May 4th, 04-05 UT): A more dense network (110-400 km, figure 11) has been used in this case because the prob-

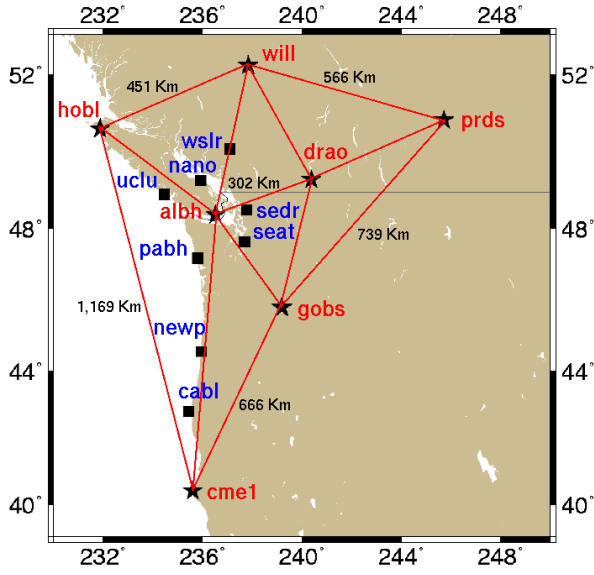


Figure 6: Map of the network of stations used for the study with moderate geomagnetic activity (stars = reference stations, squares = test stations)

lem is especially difficult due to the the rapidly changing electron density: see variation of TEC for IGS station WSLR computed directly -Hernández-Pajares et al. 1997b- in figure 12, and an example of STEC variation in figure 13. The RMS of the double differenced ionospheric residuals is 16 cm of $L_1 - L_2$ delay in this case (figure 14). And this produces a poorest determination of the widelane ambiguity. Its successful percentage is plotted against the time, a more relevant parameter in this case, in figure 15. The percentage drops from 90% to 60% from 4.3 to 4.5 hours, coinciding with the more severe variation of the geomagnetic storm (and an associated TID) as can be seen in figures 12 and 13. The results are worst without ionospheric corrections, especially in the first part.

The standard WADGPS ionospheric models typically use the smoothed pseudorange as ionospheric observable. We have also compared the ionospheric models using the carrier phase data to those using the smoothed code data. In this sense we have computed, for the scenario with moderate geomagnetic activity, the ionospheric correction using only the smoothed code data, with the same parameters that when the carrier phase is used; in particular with the same sampling period (30 seconds) and without multipath correction. With these conditions, the RMS of the double differences with the smoothed code is larger than 10 cm of $L_1 - L_2$ (a mean value of 20 cm) especially at low elevations and this is the reason to get poorest results less than 30 degrees (see figure 16).

CONCLUSIONS

We can summarize the conclusions in two main points:

1. The tomographic voxel modeling with two layers of the ionosphere provides more accurate predictions of the

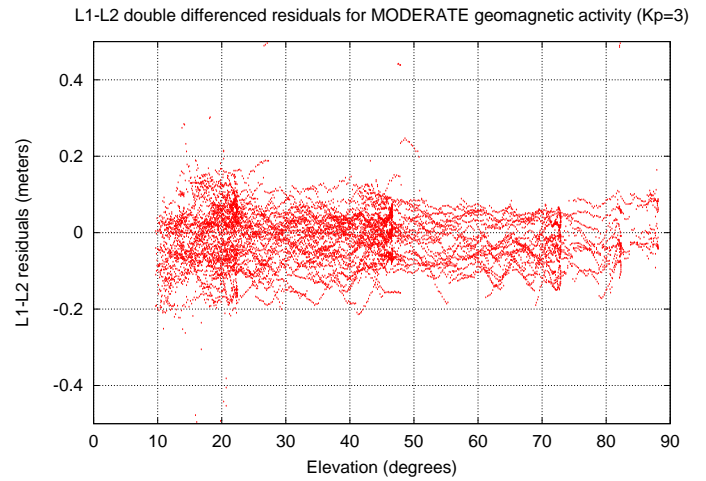


Figure 7: Double differences of the ionospheric residuals computed in the moderate geomagnetic activity scenario as a function of the non-reference satellite.

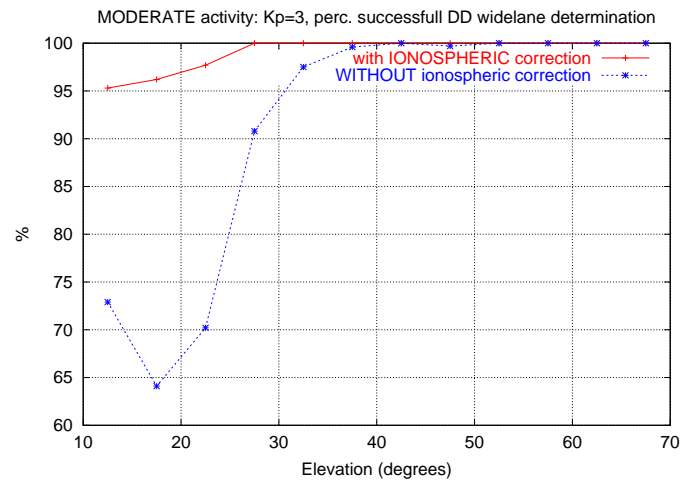


Figure 8: Percentage of successful widelane double integer ambiguity determination as a function of the elevation of the lowest satellite, for moderate geomagnetic activity (Kp=3).

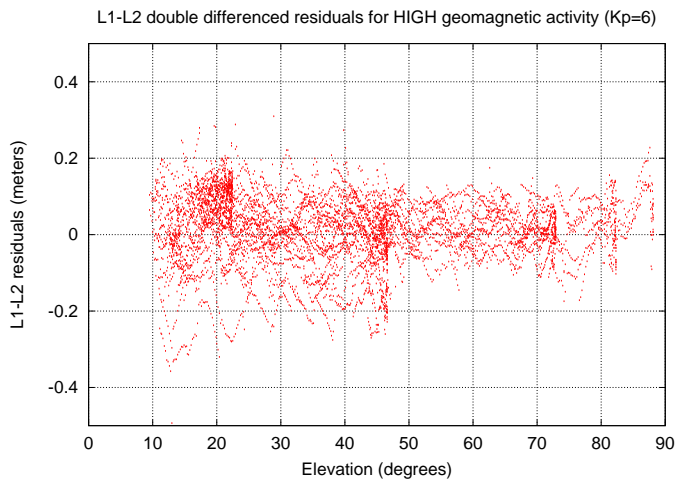


Figure 9: Double differences of the ionospheric residuals computed in the high geomagnetic activity scenario as a function of the elevation of the non-reference satellite.

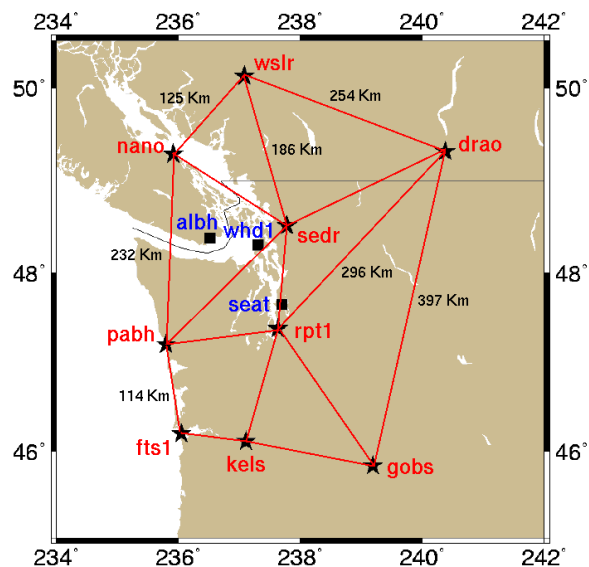


Figure 11: Map of the network of stations used for the study with large storm conditions (stars = reference stations, squares = test stations)

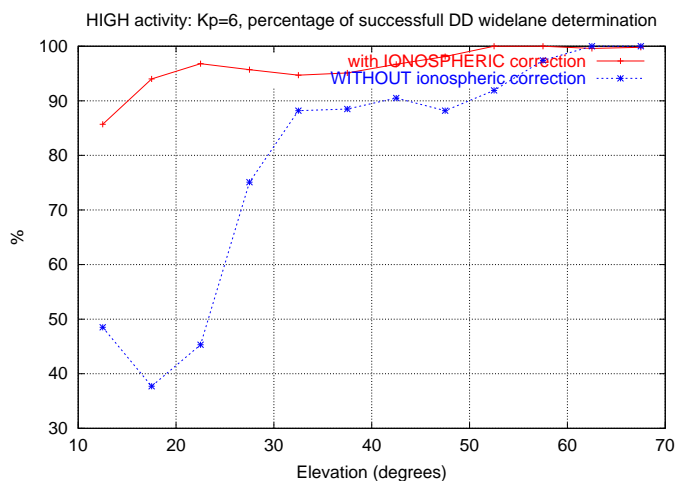


Figure 10: Percentage of successful widelane double integer ambiguity determination as a function of the elevation of the lowest satellite, for high geomagnetic activity ($K_p=6$).

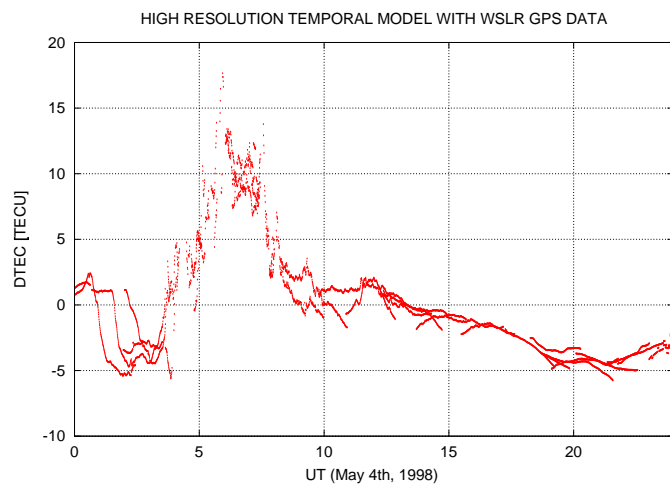


Figure 12: Variation of vertical Total Electron Content relative to the mean value for each direction in the last 7 days (DTEC) as a function of the time: IGS station WSLR during the day May 4th 1998 (a large ionospheric storm can be observed in the first part of the day).

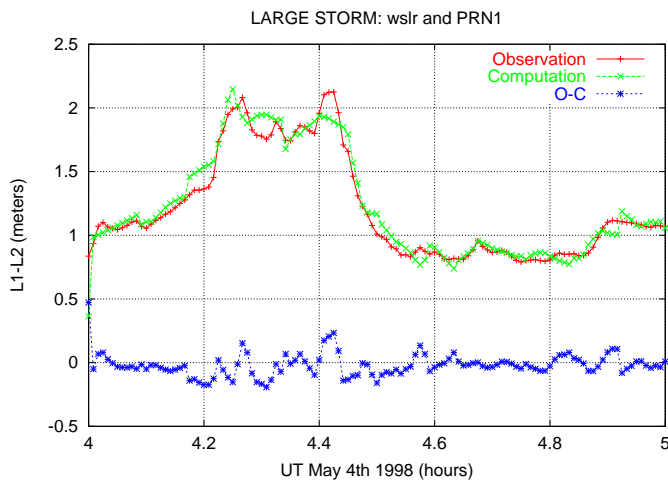


Figure 13: Predicted versus observed $L_1 - L_2$ values during the large storm happened at May 4th, 1998.

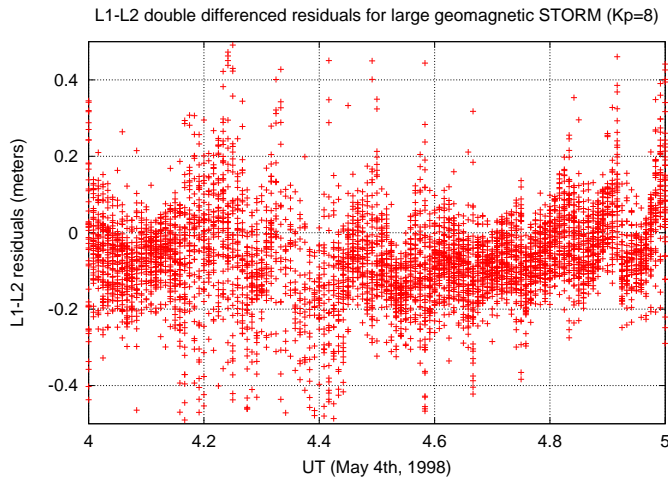


Figure 14: Double differences of the ionospheric residuals computed in the geomagnetic storm scenario as a function of the UT.

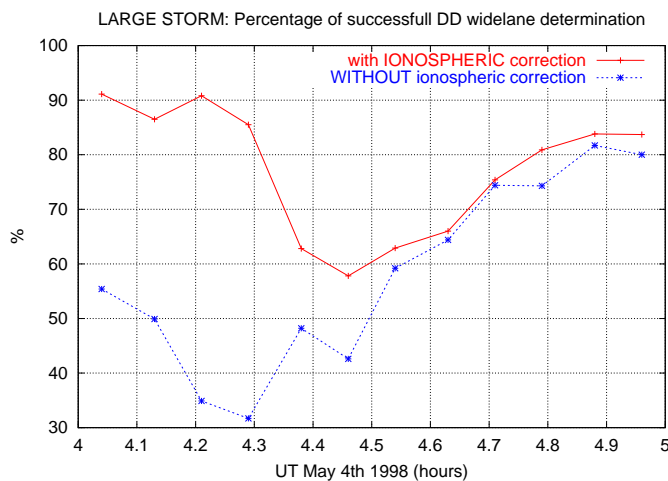


Figure 15: Percentage of successful widelane double integer ambiguity determination as a function on UT, for a large storm ($K_p=8$).

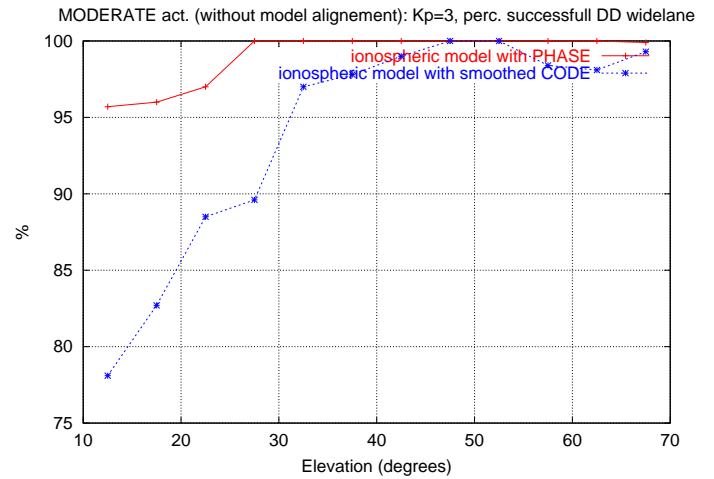


Figure 16: Percentage of successful widelane double integer ambiguity determination as a function of the elevation using the smoothed code and the carrier phase (moderate geomagnetic activity, $K_p=3$).

absolute, single and double differenced ionospheric delays than the standard fixed height layer. These results, obtained solving the model at real time, confirms the results obtained in postprocess for the Total Electron Content (Hernández-Pajares et al. 1999), in which study this difference is still more clear in equatorial regions.

2. The real time tomographic models provide enough precision, better than 1 TECU (i.e. 10 cm in $L_1 - L_2$ delay units) in the double differences of the slant TEC. This allows the successful resolution OTF of the wide lane double differenced ambiguities, also with high geomagnetic activity ($K_p=6$), and with distances up to 1300 km between reference stations. For very high geomagnetic activity ($K_p=8$) the precision of the model is not enough to solve the widelane ambiguities OTF in a satisfactory way.

ACKNOWLEDGMENTS

The authors acknowledge to the International GPS Service the availability of the real data sets. We also acknowledge to Dr. Bilitza the availability of the IRI. The maps have been generated with the software package GMT (Wessel and Smith, 1995). This work has been partially supported by the Spanish CICYT TIC97-0993-C02-01 project, and by the Spanish Ministry of Education grant PR98-0035020050.

REFERENCES

- Bierman, G.J., Factorization Methods for Discrete Sequential Estimation, Vol. 128 in Mathematics in Science and Engineering, Academic Press, New York, 1977.
- Colombo, O., M. Hernández-Pajares, J.M. Juan, J. Sanz and J. Talaya, Resolving carrier-phase ambiguities on-the fly, at more than 100 km from nearest site, with the help of ionospheric tomography, ION GPS'99, Nashville, USA, September 1999.
- Coster, A.J., M.M. Pratt, B.P. Burke and P.N. Misra, Characterization of Atmospheric Propagation Errors for DGPS, ION

54th Annual Meeting, Denver, USA, June 1998.

Enge, P., T. Walter, S. Pullen, C. Kee, Y.-C. Chao and Y.-J. Tsai, Wide area augmentation of the global positioning system, Proceedings of the IEEE, vol. 84, no. 8, p. 1063-1088, 1996.

Gao, Y., Z. Li and J.F. McLellan, Carrier phase based regional area differential GPS for decimeter-level positioning and navigation, Proceedings of the ION GPS'97, p. 1305-1313, 1997.

Hansen, A.J., Walter T., and P. Enge, Ionospheric Correction Using Tomography. Proceedings of the ION GPS '97, p. 249-257, 1997.

Hernández-Pajares, M., Juan, J.M. and Sanz, J, Neural network modeling of the ionospheric electron content at global scale using GPS data, Radio Science 32, 1081-1090, 1997a.

Hernández-Pajares, M., Juan, J.M. and Sanz, J, High-resolution TEC monitoring method using permanent ground GPS receivers, Geophysical Research Letters, 24, 1643-1646, 1997b.

Hernández-Pajares, M., Juan, J.M., Sanz, J. and Solé, J.G., Global observation of the ionospheric electronic response to solar events using ground and LEO GPS data, Journal of Geophysical Research 103, A9, 20789-20796, 1998.

Hernández-Pajares, M., Juan, J.M. and Sanz, J, New approaches in global ionospheric determination using ground GPS data, Journal of Atmospheric and Solar-Terrestrial Physics, accepted, 1999.

Niell, A.E., Global mapping functions for the atmospheric delay at radio wavelengths, Journal of Geophysical Research, 101, B2, 3227-3246, 1996.

Pratt, M., B. Burke and P. Misra, Single-Epoch Integer Ambiguity Resolution with GPS-GLONASS L1-L2 Data, ION GPS'98, Nashville, USA, September 1998.

Wessel, P. and Smith, W.H.F, New version of the Generic Mapping Tools released, EOS transactions AGU 76, 326, 1995.